# Development and Performance Evaluation of Sunflower Straw Cellulose Ether Ecological Sand-fixing Material

Ziyang Zhang,[a,b,#] Zheyu Li,[a,#] Lihong Yao,[a,b,*] Siyu Chang,[a] and Yueqi Wu [a]

Sunflowers are widely cultivated as a cash crop in the Inner Mongolia Autonomous Region, China. However, due to the lack of efficient resource utilization techniques, most of the sunflower stalks are discarded. In the Hetao irrigation area, the problem of desertification has prompted the limited use of sunflower straw to construct physical sand barriers for windbreaks and sand stabilization. In response to this, this study focuses on synthesizing a cellulose ether sand-fixing material using sunflower straw, the primary agricultural waste in Denkou County, Hetao irrigation district. This material enhances the effective adhesion between sand grains, reduces porosity among loose sand grains, and inhibits sand grain movement. The findings from this study conclusively demonstrate that the sand-fixing materials under investigation meet international standards for mechanical properties. They effectively transform loose, unconnected sand grains into a state with strong adhesion properties.

*DOI: 10.15376/biores.19.2.2201-2215*

*Keywords: Sunflower straw; Cellulose; CMC; Chemical sand fixation; Sand-fixing performance*

*Contact information: a: College of Materials Science and Art Design, Inner Mongolia Agricultural University, Hohhot 010018, Inner Mongolia, China; b: Inner Mongolia Autonomous Region Russia-Mongolia Imported Wood Processing and Utilization Engineering Technology Research Center, Hohhot 010018, Inner Mongolia, China; [#]: These authors contributed equally to this work;*
** Corresponding author: yaolihong@imau.edu.cn*

## INTRODUCTION

Desertification of land on a global scale stands as one of the pressing environmental challenges of our time, posing a substantial threat to ecosystem stability and the sustainable development of human society (Sun *et al*. 2021). This phenomenon contributes to soil erosion, diminished agricultural productivity, water resource scarcity, ecosystem degradation, and large-scale population displacement (Amin 2004). The urgency of addressing desertification is further magnified within the context of climate change, as shifting climate patterns trigger prolonged droughts and extreme weather events, exacerbating the spread of desertification (Jiang *et al*. 2014).

Conventional methods for tackling desertification and land degradation typically involve artificial water source introduction, afforestation, or the application of sand-fixing materials to stabilize dunes and desert regions. Unfortunately, these methods tend to be expensive, environmentally unsustainable, and can lead to adverse ecological consequences (Li *et al*. 2017; Martínez-Valderrama *et al*. 2020; Abdel Rahman 2023). Consequently, there is a pressing need for a more sustainable and effective approach to address this significant issue, which serves as a central driving force behind this study.

In China's Inner Mongolia Autonomous Region, sunflower is widely grown as a cash crop. The feedstock is rich in cellulose, a major component of plant cell walls and a

widely occurring renewable resource in nature (Li *et al.* 2021). However, due to the lack of effective resource reuse technologies, most of the sunflower stems are discarded. Therefore, this study envisaged the synthesis of sodium carboxymethyl cellulose from sunflower straw, having a relatively low level of substitution, which is a promising environmentally friendly material and has great potential in the production of environmentally friendly sand-fixing materials (DeLollis 1970; Gröndahl *et al*. 2021).

Carboxymethyl cellulose (CMC) is a linear polymer with ionic properties derived from natural cellulose, belonging to the class of anionic polyelectrolytes. It is one of the most widespread and important anionic polysaccharides (Suppiah *et al.* 2019). Due to its unique advantages, including low cost, high abundance, non-toxicity, biodegradability, biocompatibility, transparency, high viscosity, high adsorption capacity, and excellent film-forming ability, CMC is considered a highly promising industrial polymer. Currently, it has been widely applied in various fields such as food, biomedicine, cosmetics, and wastewater treatment (Genovese *et al.* 2014). CMC's exceptional ability to bind and retain water makes it highly valuable as a candidate material for improving soil in arid environments. The synthesis methods of CMC can be classified based on the reaction medium into two categories: water-based and solvent-based methods. The water-based method uses water as the reaction medium and is suitable for producing alkaline and low-grade CMC. The solvent-based method employs organic solvents as the reaction medium and is applicable for the synthesis of medium to high-grade CMC. The preparation process for both methods involves two stages: alkalization of cellulose and etherification of alkalized cellulose (cellulose etherification) (Huang *et al.* 2009). For instance, Mingkun Yang synthesized carboxymethyl cellulose sodium (CMC) sand-fixing agent using corn husks and straw as raw materials through a solvent-based method with a two-step alkalization process (Yang, 2012). CMC that has a sufficiently high degree of substitution is a water-soluble cellulose colloid, and its viscosity depends on the degree of carboxymethylation. The degree and uniformity of carboxymethylation can be controlled through preparation processes and reaction conditions, which are reflected in its rheological behavior in solution (Elliot and Ganz 1974).

The primary goal of this study was to develop eco-friendly sand-fixing material based on cellulose from sunflower stalk and conduct a comprehensive evaluation of their properties. Experimental methods to assess the structure and sand-fixing characteristics of this novel material were designed. The wider objective of this study was to offer a sustainable solution to combat land degradation and sand-fixing challenges, while also making a valuable contribution to the advancement and adoption of environmentally friendly materials.

## EXPERIMENTAL

### Materials

Sunflower straw was sourced from Dengkou County, Bayannur City, Inner Mongolia Autonomous Region, ensuring the selection of materials were free from mold and obvious defects. The following reagents and substances were used in the experiment.

Nitric acid from Sinopharm Group Chemical Reagent Co., Ltd., sodium hydroxide and glacial acetic acid from Fuchen (Tianjin) Chemical Reagent Co., Ltd., sodium hypochlorite and sodium chloroacetate from Tianjin Fuyu Fine Chemical Co., Ltd., and anhydrous ethanol from Yongfei Chemical Reagent Co., Ltd. were used as received.

The sand used (40 to 120 mesh) was obtained from the Tengger Desert, and distilled water was prepared in the laboratory.

This study utilized the following characterization instruments: the TESCAN-MIRA-LMS model scanning electron microscope (SEM) manufactured by Tesken Co., Ltd. in Shanghai, China; the IR-Tracer-100 model Fourier-transform infrared spectrometer (FTIR) produced by Shanghai Yanrun Optical Machine Technology Co., Ltd. in Shanghai, China; the SmartLab-SE model X-ray diffractometer (XRD) manufactured by China's Physicochemical Syce Technology Co., Ltd. in Beijing, China; and the NetzschSTA449F5 model thermogravimetric analyzer (TG) produced by Shenzhen Blue Star Yu Electronic Technology Co., Ltd. in Shenzhen, China.

## Methods

Figure 1 illustrates the technical flow diagram to produce sodium carboxymethyl cellulose used for sand fixation. The process can be broken down into the following steps.

*Preparation of sunflower straw powder*

Harvested sunflower stalks were thoroughly dried in an electric thermostatic air-drying oven at 105 ± 2 ℃. The dried stalks were divided into 10 to 15 cm sections, and the xylem and pulp are manually separated. The separated sunflower stalk xylem was washed with distilled water to remove surface impurities and then dried at 105 ± 2 ℃ for 6 h The resulting material, referred to as sunflower straw powder (SFSP), was obtained by crushing and sifting the dried xylem through a 40- to 60-mesh sieve.

*Preparation of sunflower straw powder holocellulose (CH-SFSP)*

Approximately 40 to 60 g of SFSP was subjected to $HNO_3$ treatment. The residue obtained after filtration was washed under negative pressure until neutral state and then vacuum dried at 105 ± 2 ℃ for 6 h to obtain acid-treated sunflower straw cellulose.

*Preparation of sunflower straw powder crude fiber (CF-SFSP)*

Cellulose from the acid-treated sunflower straw was then used as the raw material. A total of 2 g of the raw material was mixed with 30 mL (6%) NaOH solution at 50 ℃ for 1 h. The sunflower straw crude cellulose obtained was filtered under negative pressure.

*Preparation of sunflower straw powder cellulose (C-SFSP)*

A 1% sodium hypochlorite solution (pH adjusted to 4/5 with glacial acetic acid) was used under specific agitation conditions for 0.5 h. After filtration under negative pressure, the filter residue was washed to a neutral state and dried at 105 ± 2 ℃ to constant weight, resulting in sunflower stem cellulose (C-SFSP).

*Preparation of sodium carboxymethyl cellulose (CMC-SFSP)*

About 4 g of sunflower straw cellulose raw material was placed in 80 mL of ethanol at 28 ℃ for 30 min. Then, 10 mL of 50% NaOH aqueous solution was added, and the mixture was allowed to react at 30 ℃ for 60 min. Subsequently, 10 mL of 40% sodium chloroacetate solution was added, and the temperature was raised to 45 ℃ for 3 h. After the reaction, the aqueous solution was made neutral with glacial acetic acid, washed with water and alcohol, and centrifuged to obtain sodium carboxymethyl cellulose.

*Preparation of sand cake*

An amount of 60 g of sand was placed in a cylindrical mold. To this 15 mL of a sand control solution with different solid contents was added, the sand and the material were then mixed thoroughly. The mixture was made compact and levelled, and then dried at 60 °C for 24 h to obtain a 5 cm diameter sand cake.

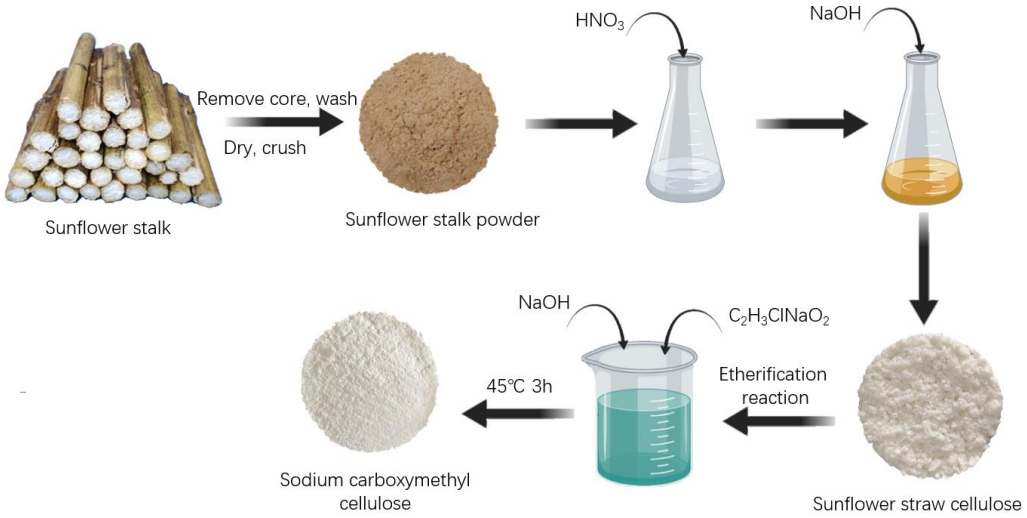


**Fig. 1.** Preparation method of sodium carboxymethyl cellulose

## RESULTS AND DISCUSSION

### Morphological Characterization

Figure 2 presents the images of sunflower culm at different stages: (a) SFSP, (b) CH-SFSP, (c) CF-SFSP, and (d) C-SFSP. The apparent color of the sunflower culm raw material underwent a noticeable transformation. It shifted from an earthy yellow hue to beige, then to light yellow, and ultimately to white. This change can be attributed to the sequential treatments. The $HNO_3$ treatment primarily removed most of the lignin and hemicellulose, while in the NaOH- and NaClO-treatment steps destroyed most of the chromophore groups present in the sunflower stalk raw material, resulting in the final white color of the product.


**Fig. 2.** Pretreatment sample diagram: (a) SFSP, (b) CH-SFSP, (c) CF-SFSP, and (d) C-SFSP

Figure 3 presents scanning electron microscopic (SEM) analyses of various samples, including sunflower stalk (Fig. 3a), sunflower stalk cellulose (Fig. 3b), and sunflower stalk-based sand-fixing material (Fig. 3c). The surface structure of the raw sunflower stalk material appeared stable, closely arranged, and contains impurities, with closed pores. Post-extraction *via* pretreatment, the surface became smoother, with smaller wrinkles and open pores, displaying a porous quality. This transformation can be attributed to the removal of surface impurities, elimination of lignin and hemicellulose, and the exposure of cellulose, resulting in higher cellulose purity within the raw sunflower stalk material. This heightened purity is beneficial for subsequent cellulose modification and application.

In Fig. 3c, the SEM of sunflower stalk cellulose ether reveals a smooth surface with a porous clustered fiber structure. After etherification modification, this bundled structure had become disrupted, and sunflower stalk cellulose ether adopted a block-like structure with a rough surface, resembling curly sheet-like structures. These characteristics are indicative of carboxymethyl cellulose sodium salt and suggest a relatively high degree of carboxymethylation in the prepared sunflower stalk cellulose ether. However, based on the images, the degree of substitution was insufficient to make the material soluble in water.

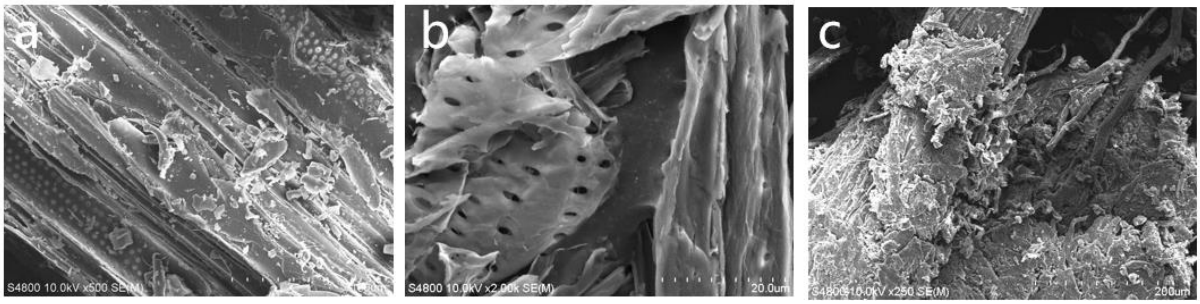


**Fig. 3.** SEM image: (a) sunflower stem raw material, (b) sunflower straw cellulose, and (c) sunflower straw cellulose ether

## Structure Characterization

Figure 4(a) presents the results of infrared spectroscopic analysis conducted on raw sunflower stalks, sunflower stalk comprehensive cellulose, sunflower stalk crude cellulose, and sunflower stalk cellulose. The absorbance characteristics in the infrared spectra of the raw material are remarkably consistent with those observed after pretreatment. This suggests that the pretreatment process primarily involves the removal of lignin and hemicellulose, as it does not induce significant structural changes in the cellulose itself. In the spectra, the peak at 3395 $cm^{-1}$ corresponds to the stretching vibration of the -OH functional group, while the peak at 2902 $cm^{-1}$ is associated with the stretching vibrations of the $-CH_3$ and C-H functional groups. Additionally, near 1429 $cm^{-1}$, there is a stretching vibration peak corresponding to the C-O-C cyclic structure in cellulose (Wang *et al*. 2017). Characteristic absorbance peaks of cellulose emerged at 1055 $cm^{-1}$ and 897 $cm^{-1}$ (Bao *et al*. 2023). In the raw sunflower stalk sample, there was an asymmetric contraction vibration peak of the carbonyl group at 1741 $cm^{-1}$. Post-pretreatment, this carbonyl peak disappeared, signifying the effective removal of most of the lignin from sunflower stalks. This indicates a relatively high extraction rate of cellulose with minimal impact on the cellulose structure because of the pretreatment process. Moreover, the pretreatment effectively removed most of the lignin and hemicellulose, resulting in a higher purity of sunflower stalk cellulose.

Figure 4(b) showcases the results of infrared spectroscopic analysis performed on C-SFSP and CMC-SFSP. Notably, a peak near 1429 $cm^{-1}$ corresponds to the stretching vibration of the C-O-C cyclic structure present in cellulose. Characteristic absorbance peaks for cellulose are clearly identified at 1068 $cm^{-1}$ and 895 $cm^{-1}$. Following the etherification modification, along with the cellulose characteristic peaks, new peaks emerged near 1372 and 1068 $cm^{-1}$. These correspond to the asymmetric and symmetric stretching vibrations of the -COONa group within sunflower stalk cellulose (Heinze and Pfeiffer 1999). These observations suggest that cellulose molecules had reacted with the etherifying agent, leading to the replacement of hydrogen on the hydroxyl group in the molecule with a carboxymethyl group.

Figure 4(c) displays the thermogravimetric analysis of C-SFSP and CMC-SFSP. The figure reveals that sunflower stalk cellulose initiated decomposition at 235 °C, exhibiting a higher thermal decomposition temperature in comparison to sunflower stalk cellulose ether. The peak rate of thermal degradation occurred between 290 and 364 °C, with a residual amount of only 0.25% by the end, nearly approaching zero. This outcome indicates the successful removal of impurities, such as lignin and hemicellulose, from sunflower stalk cellulose, resulting in a high degree of cellulose purity.

In contrast, CMC-SFSP demonstrated a lower thermal decomposition initiation temperature at 199 °C. The peak rate of thermal degradation occurred between 225 and 304 °C, with a subsequent reduction in the extent of thermal decomposition between 304 °C and 800 °C. This suggests excellent thermal stability of CMC-SFSP. At 800 °C, the residual amount decreased to 25.1%, implying the absence of carbon and sodium compounds.

Figure 4(d) exhibits images from X-ray diffraction (XRD) analysis of SFSP, CH-SFSP, CF-SFSP, and C-SFSP. The diffraction peaks in each sample remained consistent both before and after pretreatment, with changes primarily observed in diffraction intensity and crystallinity. However, the cellulose crystal structure remained unaffected, signifying that the pretreatment exerted minimal impact on the cellulose. Prominent diffraction peaks were observed near $2\theta = 22.5°$ and $2\theta = 17°$, corresponding to the (002) and (101) crystal planes of cellulose I (Li *et al*. 2019). The crystallinity of cellulose in the sample experienced a significant increase. This suggests that the removal of lignin and hemicellulose components from sunflower stalk during pretreatment was effective, and the enhancement in crystallinity was most pronounced following $HNO_3$ treatment, surpassing that observed with NaOH and NaClO treatments. These findings corroborate the conclusions drawn from SEM images and affirm a substantial increase in cellulose purity within the raw material post-nitric acid treatment, aligning with the results of this experiment.

Figure 4(e) presents the XRD patterns of C-SFSP and CMC-SFSP. During the carboxymethylation modification of sunflower stalk cellulose, the diffraction peak at $2\theta = 15°$ gradually shifted to lower angles, becoming broader and less intense. At $2\theta = 22.5°$, a new diffraction peak corresponding to the (002) crystal plane of cellulose I emerged. In contrast, in the XRD pattern of sunflower stalk cellulose ether, the diffraction peak at $2\theta = 15°$ nearly disappeared, and a new crystalline peak appears at $2\theta = 20°$. This reflects a transition in the cellulose crystal type from cellulose I to cellulose II, indicating changes in the cellulose crystal structure and internal molecular rearrangement.

The etherification process weakened the hydrogen bonding of cellulose, and the degree of carboxymethylation was relatively high. The synthesized sunflower stalk cellulose ether exhibited high viscosity, aligning with the findings of this study.

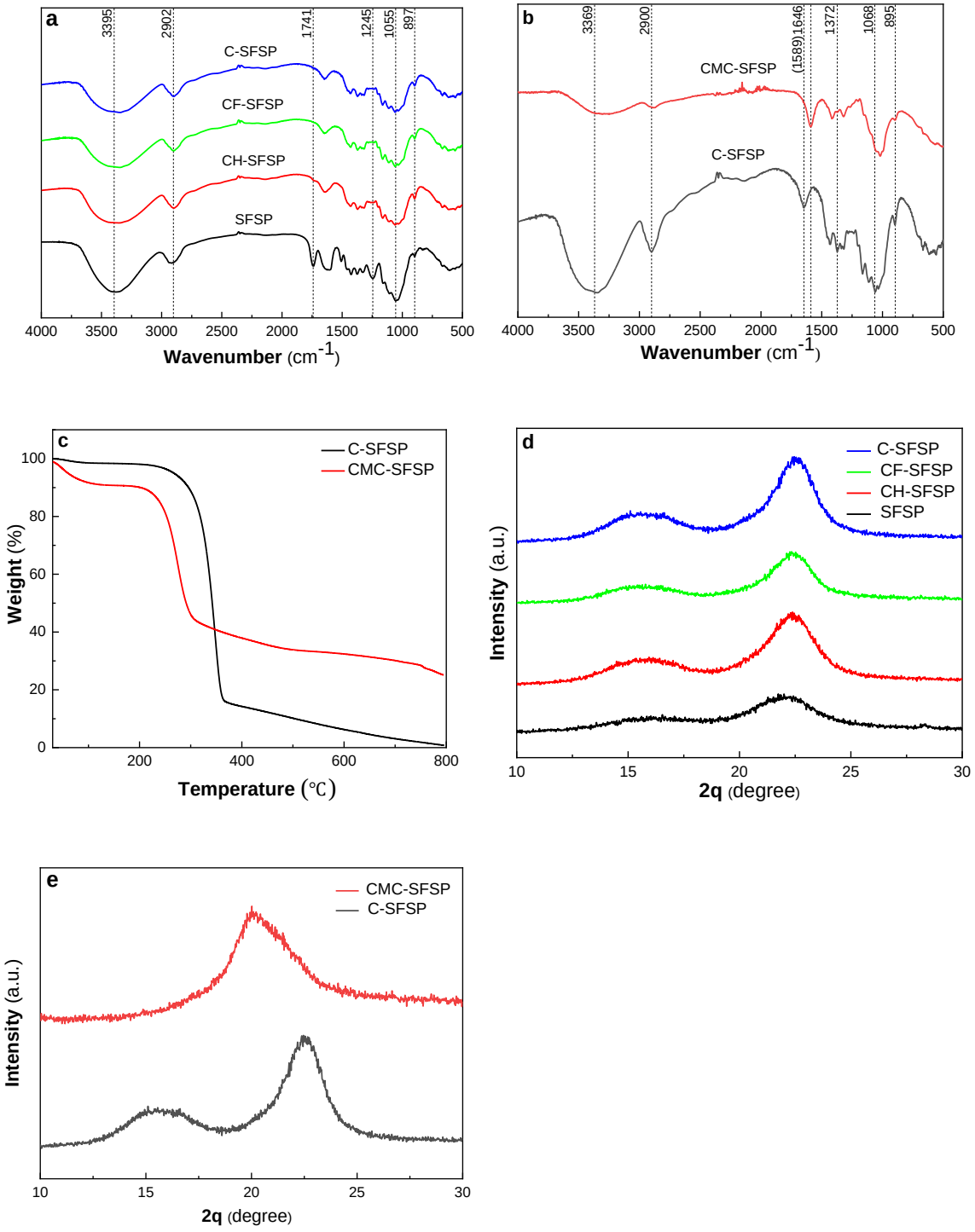


**Fig. 4.** (a), (b) Infrared spectra; (c) thermogravimetric analysis; (d), (e) XRD analysis patterns for C-SFSP and CMC-SFSP samples

## Application Performance Test

First, samples of CMC-SFSP with varying solid contents were prepared. This method was utilized for producing the sand cake and assessing its properties, including

compressive strength, structural morphology, water retention, aging resistance, UV aging resistance, freeze-thaw aging resistance, salt-alkali resistance, and degradation resistance.

*Compressive strength analysis*

Figure 5 provides representative illustrations of sand cakes prepared with different solid contents following compressive strength testing. The inherent plasticity of the sand cake results in buffering forces during testing, maintaining its original basic shape. The compressive strength of the sand cake was determined through testing in a universal mechanical testing machine, with the stress peak recorded as the basis for assessing the compressive strength.

In Fig. 6(a), the variation in the compressive strength of sand cakes with respect to the solid content changes of the CMC-SFSP water-soluble solution. As the solid content increased, the compressive strength of the sand cakes consistently rose, demonstrating a positive correlation. This is attributed to the increased viscosity of the solution within the sand mixture as the solid content increases, which enhanced the binding and adhesion between sand particles, resulting in an increased compressive strength. At a solid content of 1.5%, the compressive strength of the sand cake reached 0.74 MPa, close to 1.0 MPa, and at 2%, the compressive strength reached 1.46 MPa, making it suitable for desertification control.

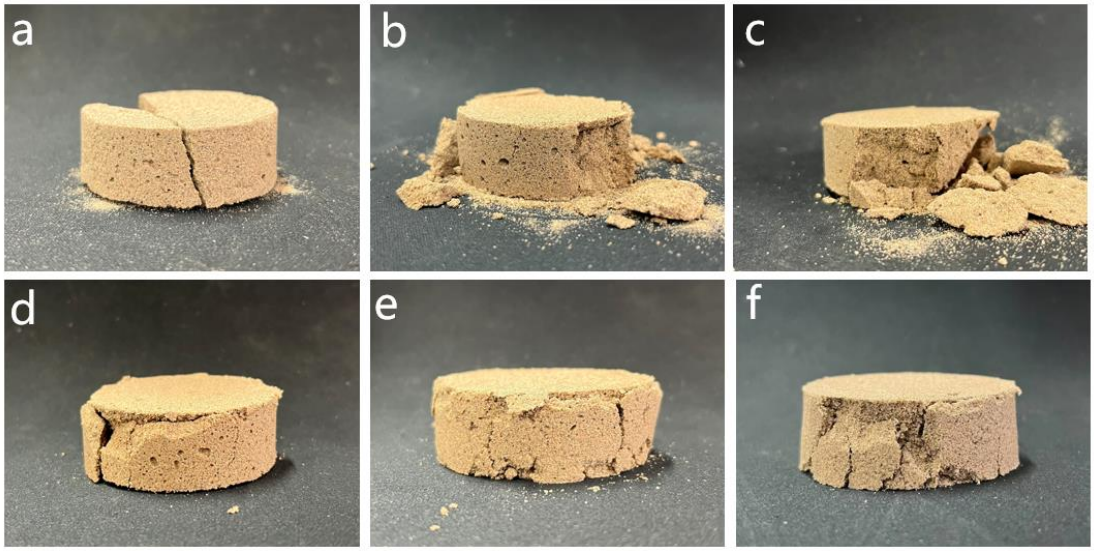


**Fig. 5.** Sample destruction diagram: (a) Solid content at 0%; (b) 0.5% solid content; (c) 1.0% solid content; (d) 1.5% solid content; (e) 2% solid content; and (f) 2.5% solid content

*Water-retaining property*

Figure 6(b) depicts the change in moisture content of sand cakes over time, which reflects the water retention capacity of the solid sand material. The rate of moisture loss was inversely related to the material's water retention capacity. During the initial 3 to 5 h, the moisture content decreased most rapidly, with a 15.4% reduction throughout the dehydration process. Subsequently, the rate of moisture content reduction gradually slowed down, with reductions of 7.3 and 5.0% between 24 to 36 h, indicating a gradual stabilization. This indicates that the solid sand material possessed a certain level of water retention capacity, with better performance observed within the first 12 h.

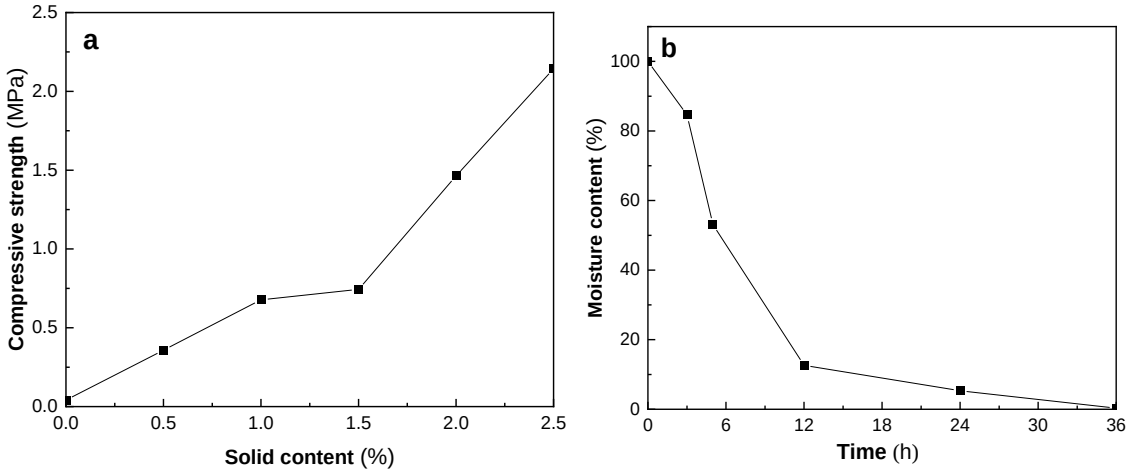


**Fig. 6.** (a) Curve of compressive strength changing with solid content: (b) Sand cake moisture content curve over time

*Morphology characterization of intergranular binding*

Figure 7 shows a schematic illustration of a sand cake prepared by mixing sand with a 2% solid content C-SFSP-based sand control solution. The sand cake had a diameter of 5 cm and a thickness of approximately 0.7 cm. It can be observed that under the influence of the sand control material, the sand grains bonded together to form a stable block-like structure.

Figure 8 provides SEM images of sand and a 2% solid content sand control water-soluble solution mixed and dried to create sand cakes. When no sand control water-soluble solution was applied, there was no physical or chemical adhesion or binding between the sand grains, resulting in a higher porosity, and the grains behaving as separate particles (as seen in Figs. 7a and 7b). However, when the sand control water-soluble solution was applied, chemical bonding occurred between the sand grains, forming an irregular physical network structure, which effectively reduced the movement of sand grains on the surface.

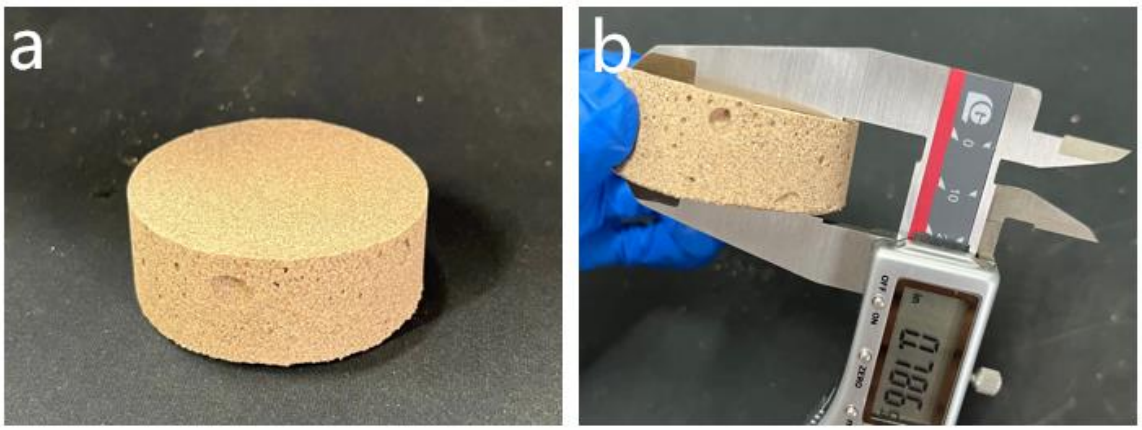


**Fig. 7.** Sand cake diagram: (a) a general picture of sand cake; (b) overall thickness of sand cake

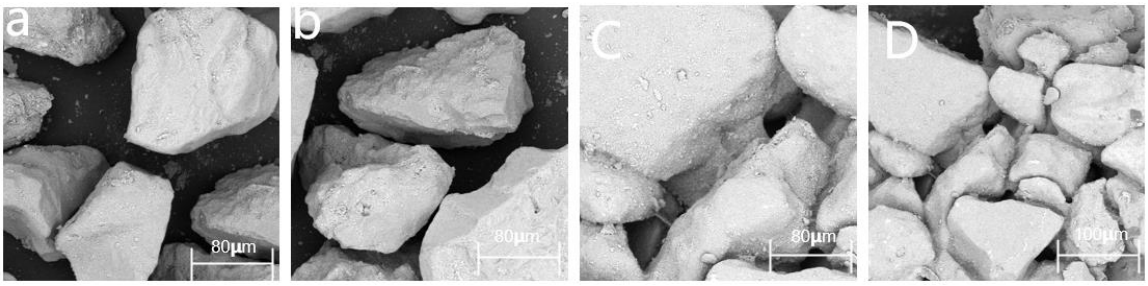


**Fig. 8.** SEM image of sand cake: (a), (b): Sand cake with 0% solid content; and (c), (d): Sand cake with 2% solid content

*Thermal aging property*

Figure 9(a) illustrates the change in compressive strength of sand cakes over the course of heat aging. With increasing aging duration, the compressive strength gradually decreased, and the rate of decrease also diminished over time. The initial compressive strength of 1.46 MPa decreased to a final value of 0.80 MPa. After 5 days of heat aging treatment, the compressive strength decreased relatively rapidly, reaching a critical value of 0.89 MPa at 10 days. This is likely attributable to changes in the molecular structure within the solid sand material at 60 °C over time, leading to some disruption in viscosity characteristics and a relative loosening of the sand cake structure, resulting in reduced compressive strength.

*Ultraviolet aging property*

Figure 9(b) illustrates the change in compressive strength of sand cakes under UV aging treatment. As the duration of UV aging increased, the compressive strength decreased from 1.46 to 0.9 MPa. The initial decrease in compressive strength was relatively rapid. At specific measurement points corresponding to UV aging times of 3 days, 5 days, 10 days, 15 days, and 20 days, the compressive strength measured 1.31 MPa, 1.25 MPa, 1.13 MPa, 1.01 MPa, and 0.9 MPa, respectively.

Remarkably, the sand cake maintained a compressive strength greater than 1.0 MPa even at 15 days, indicating robust UV aging resistance in the solid sand material. The rate of compressive strength decline was faster initially but gradually slowed down in the later stages. This behavior may be attributed to the impact of UV radiation on the molecular structure of the sand cake, resulting in gradual changes and disruptions, leading to a progressive reduction in compressive strength over time.

*Degradability*

Figure 9(c) illustrates the change in the mass of the sand cake within the soil over time. As time progressed, the mass loss gradually increased, signifying the biodegradable nature of the solid sand material. At various time points, including 3 days, 5 days, 10 days, 15 days, and 20 days, the measured mass loss percentages were 1.53%, 1.7%, 1.88%, 1.98%, and 2.09%, respectively.

The figure demonstrates that the material degraded more slowly during the initial stages and accelerated in the later stages. This behavior is likely due to the combined influence of physical, chemical, and biological processes in the environment, which induce changes and disruptions in the molecular structure of the solid sand material and subsequently enhance the degradation rate.

*Freeze-thaw aging*

Figure 9(d) presents the trend of compressive strength changes in sand cakes subjected to varying freeze-thaw aging treatment cycles. It is evident that, as freeze-thaw aging time increased, the compressive strength of the material gradually diminished, declining from 1.46 to 0.8 MPa. During the initial 10 days, the decrease in compressive strength was relatively gradual, but after 10 days, the decline accelerated markedly. By the 20$^{th}$ day, the extent of compressive strength reduction notably increased, with the compressive strength at the 15$^{th}$ day measuring 1.04 MPa, indicating robust resistance to freeze-thaw aging in the solid sand material. Overall, there was a consistent decreasing trend in compressive strength.

This behavior can be attributed to the increased moisture infiltrating the material's interior, leading to the formation of ice crystals with a greater number of freeze-thaw cycles. Consequently, this elevated internal stress within the material, causing microstructural damage and cracks that resulted in reduced compressive strength. As the number of cycles increased, the rate of the compressive strength decline gradually slowed down, likely due to internal modifications in the sand cake, imposing certain constraints on the reduction in compressive strength.

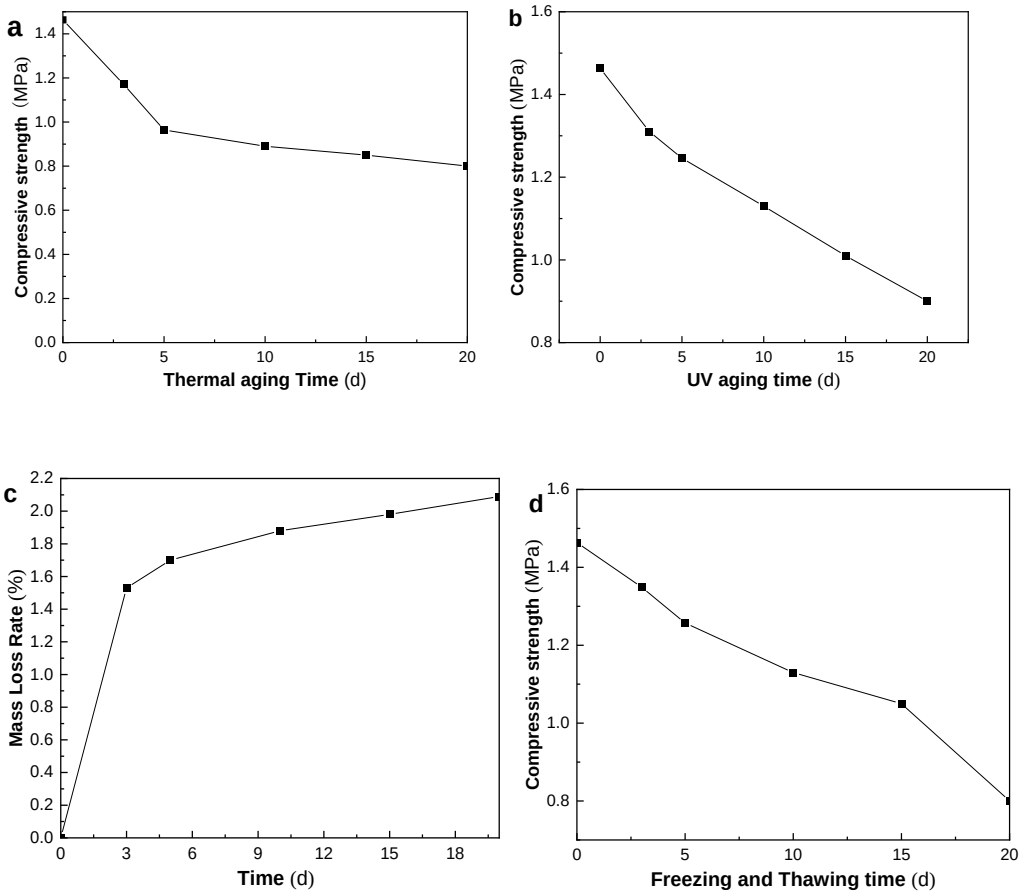


**Fig. 9.** (a) Sand cake with a solid content of 2 % for materials curve of compressive strength with thermal aging time; (b) Sand cake with a solid content of 2 % for materials curve of compressive strength with UV aging time; (c) Sand cake with a solid content of 2 % for materials curve of sand cake mass loss rate over time; and (d) Sand cake with a solid content of 2 % for materials curve

of compressive strength variation with freeze-thaw aging time

*Resistant to saline-alkali acid*

Figure 10 depicts the transformations observed in sand cakes when exposed to water, salt, alkali, and acidic solutions. Notably, the mechanical properties of the sand cakes were compromised in water and alkali solutions, leading to a loosening of the sand cake structure. This highlights a lack of water resistance and alkali resistance in the material. In contrast, the sand cakes maintained their original form when placed in salt and acidic solutions.

The sandcakes were initially immersed in various solutions, including aqueous (Fig. 10a), salt (Fig. 10b), alkaline (Fig. 10c), and acid (Fig. 10 d) solutions. Subsequently, they were left for extended periods, including 24 h (Figs. 10e, 10f, 10g, 10h) and even 48 h (Figs. 10i, 10j, 10k, 10l) within salt and acid solutions. Notably, the shape of the sandcakes remained largely unaltered throughout these exposure periods. This robust performance suggests that the solid sand material can exhibit exceptional resistance to salt and acid, underscoring its durability in these challenging environmental conditions.

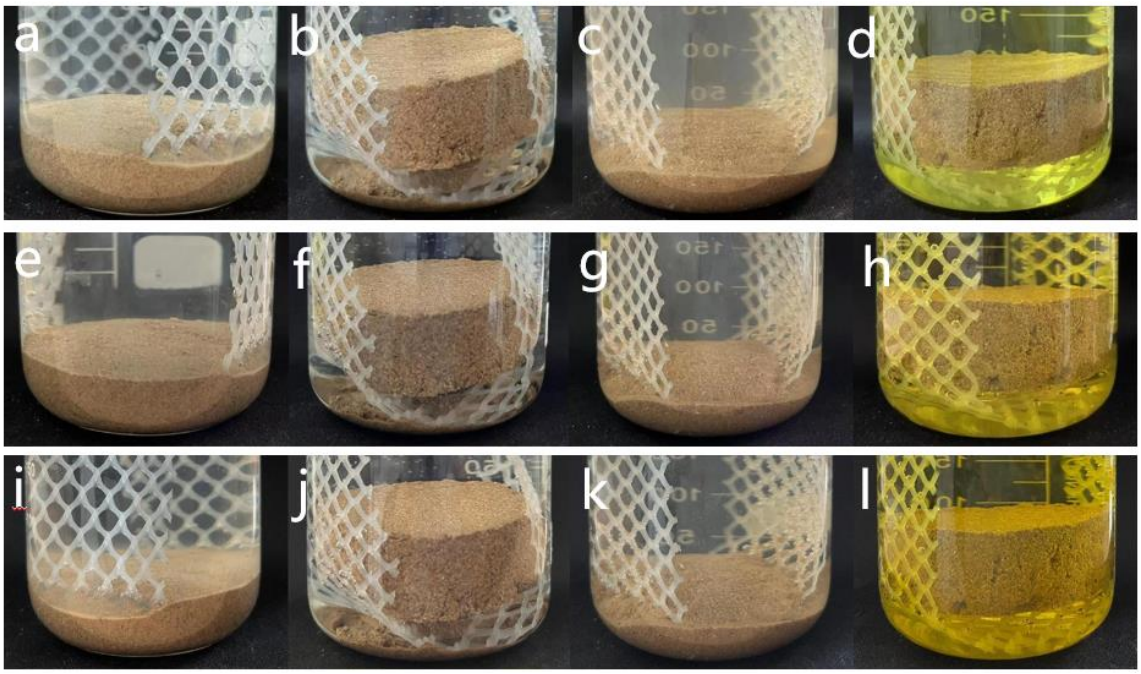


**Fig. 10.** The change of sand cake with solid content of 2 % in water, salt, alkali and acid solution.: (a), (e), (i) Sand cake in aqueous solution; (b), (f), (j) sand cake in salt solution; (c), (g), (k) sand cake in alkali solution; and (d), (h), (l) sand cake in acid solution

*Biocompatibility*

As shown in Fig. 11, after spraying the water-soluble solid sand control material, there were no adverse changes in the plant growth condition. In comparison to the control sprayed with water, the growth was healthier. The photos of plant growth, it can be found that plants grew better after adding CMC. It is possible that the presence of CMC will increase the moisture content of the soil in equilibrium. This indicates that the solid sand control material exhibited excellent biocompatibility and contributed to promoting plant growth. This not only helps address desertification issues but also has the potential to improve desert soil.

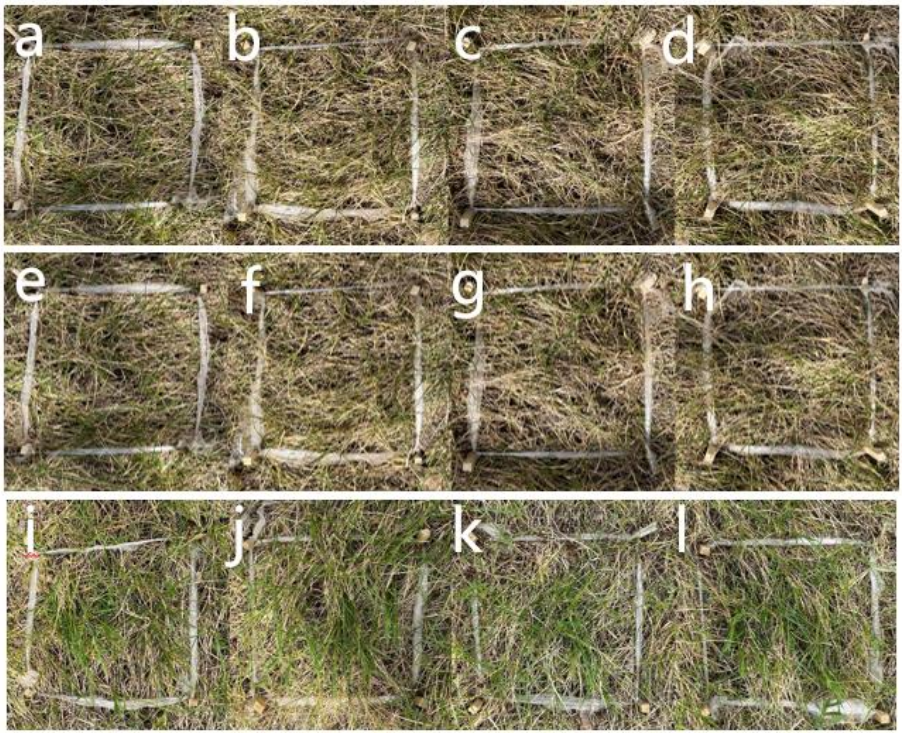


**Fig. 11.** Changes of plant growth before and after spraying CMC solution with solid content of 2 %.: (a), (e) The blank control; (b), (c), (d) the growth of sand fixation solution sprayed for 0 days; (f), (g), (h) the growth of sand fixing solution sprayed for 5 days; and (f), (g), (h) the growth of sand fixing solution sprayed for 30 days

## CONCLUSIONS

1. This study utilized discarded sunflower stalks as raw material, removing hemicellulose and lignin, and successfully preparing the corresponding carboxymethyl cellulose (CMC-SFSP) through cellulose etherification. The prepared CMC-SFSP was applied to sand fixation technology.
2. The results indicate that the method used to remove lignin and hemicellulose in this experiment did not affect the crystalline form and crystalline region of cellulose. Infrared analysis confirmed the successful removal of hemicellulose and lignin. After cellulose etherification modification, the internal molecular structure of sunflower stem cellulose was transformed from cellulose I to cellulose II. Characteristic features of carboxymethyl cellulose sodium salt were observed under SEM, exhibiting significant resistance to degradation below 200 °C and excellent thermal stability.
3. Upon mixing CMC material with sand, a shift in the bonding pattern between sand particles was observed. Under the influence of the sand-fixing material, sand particles transitioned from a loose, independent structure to a physically bonded network structure. This transformation significantly reduced the porosity between sand particles. The material's compressive strength, resistance to aging, freeze-thaw resistance, and heat aging resistance were investigated, revealing that these properties were all relatively good.

4. This provides a novel pathway for the recycling of discarded sunflower stalks. The synthesized CMC demonstrated excellent sand-fixing effects.
5. The future wind and sand fixation materials should be studied in the direction of more environmental protection and more efficient.

## ACKNOWLEDGMENTS

The authors are grateful for the support of the National Natural Science Foundation of China (32360356), Inner Mongolia grassland talent team, and innovative talent team (Tc2019071720712).

## REFERENCES CITED

Abdel Rahman, M. A. (2023). "An overview of land degradation, desertification and sustainable land management using GIS and remote sensing applications," *Rendiconti Lincei. Scienze Fisiche e Naturali* 34, 767-808. DOI: 10.1007/s12210-023-01155-3

Amin, A. A. (2004) "The extent of desertification on Saudi Arabia," *Environmental Geology* 46, 22-31. DOI: 10.1007/s00254-004-1009-0

Bao, G. R., Cheng, S. R. N., Ling, X., Bao, S. D., Ha, S., and Li, F. Q. (2023). "Optimization of cellulose extraction from buckwheat straw by Box-Behnken response surface method," *Chemical Research and Application* 3, 532-538.

DeLollis, N. J. (1970). "Theory of adhesion, mechanism of bond failure, and mechanism for bond improvement," *Rubber Chemistry and Technology* 43(2), 229-243. DOI: 10.5254/1.3547250

Elliot, J., and Ganz, A. (1974). "Some rheological properties of sodium carboxymethylcellulose solutions and gels," *Rheologica Acta* 13, 670-674. DOI: 10.1007/bf01527058.

Genovese, M., Viccione, F., and Rossi, D. (2014). "Using the sodium carboxymethyl cellulose (CMC) as viscosity modifier to model the interstitial fluid in laboratory debris flows," *Eng Geol* 26, 179-186.

Gröndahl, J., Karisalmi, K., and Vapaavuori, J. (2021). "Micro-and nanocelluloses from non-wood waste sources; processes and use in industrial applications," *Soft Matter* 17(43), 9842-9858. DOI: 10.1039/d1sm00958c

Heinze, T., and Pfeiffer, K. (1999). "Studies on the synthesis and characterization of carboxymethylcellulose," *Die Angewandte Makromolekulare Chemie* 266(1), 37-45. DOI: 10.1002/(SICI)1522-9505(19990501)266:1<37::AID-APMC37>3.0.CO;2-Z

Huang, B., Hong, J.-Y., and Wang, M.-R. (2009). "Screening and identification of cellulose-degradation strain M1 and its characteristics of cellulase," *Journal of Life Science* 3, 21-26.

Jiang, Z., Lian, Y.-Q., and Qin, X.-Q. (2014). "Rocky desertification in Southwest China: Impacts, causes, and restoration," *Earth-Science Reviews* 132, 1-12. DOI: 10.1016/j.earscirev.2014.01.005

Li, H., Zhang, H., Xiong, L., Chen, X., Wang, C., Huang, C., and Chen, X. (2019). "Isolation of cellulose from wheat straw and its utilization for the preparation of

carboxymethyl cellulose," *Fibers and Polymers* 20, 975-981. DOI: 10.1007/s12221-019-7717-6

Li, T., Chen, C., Brozena, A. H., Zhu, J. Y., Xu, L., Driemeier, C., Dai, J., Rojas, O. J., Isogai, A., Wågberg, L., *et al.* (2021). "Developing fibrillated cellulose as a sustainable technological material," *Nature* 590(7844), 47-56. DOI: 10.1038/s41586-020-03167-7

Li, Y., Li, Z., Wang, Z., Wang, W., Jia, Y., and Tian, S. (2017). "Impacts of artificially planted vegetation on the ecological restoration of movable sand dunes in the Mugetan Desert, northeastern Qinghai-Tibet Plateau," *International Journal of Sediment Research* 32(2), 277-287. DOI: 10.1016/j.ijsrc.2017.02.003

Martínez-Valderrama, J., Guirado, E., and Maestre, F. T. (2020). "Desertifying deserts," *Nature Sustainability* 3(8), 572-575. DOI: 10.1038/s41893-020-0561-2

Sun, X.-H., Miao, L.-C., Wang, H.-X., Wu, L.-Y., and Zhang, J.-Z. (2021). "Enzymatic calcification to solidify desert sands for sandstorm control," *Climate Risk Management* 33, article ID 100323. DOI: 10.1016/J.CRM.2021.100323

Suppiah, K., Leng, T. G., and Husseinsyah, S. (2019). "Thermal properties of carboxymethyl cellulose (CMC) filled halloysite nanotube (HNT) bio-nanocomposite films," *Materials Today* 16, 1611-1616. DOI: 10.1016/j.matpr.2019.06.025.

Wang, N., Li, R. Y., Li, G., and Zhang, S. (2017). "Optimization of extracting technology for coffee cellulose and characterization of its microstructure," *Chemical Industry and Engineering Progress* 2017(06), 2262-2269. DOI: 10.16085/j.issn.1000-6613.2017.06.042

Article submitted: October 21, 2023; Peer review completed: November 27, 2023; Revised version received and accepted: December 14, 2023; Published: February 18, 2024.
DOI: 10.15376/biores.19.2.2201-2215